Acta Crystallographica Section D
Biological Crystallography
ISSN 0907-4449

Structure determination of the *O*-methyltransferase NovP using the 'free lunch algorithm' as implemented in *SHELXE*

Isabel Usón,[a]* Clare E. M. Stevenson,[b] David M. Lawson[b] and George M. Sheldrick[c]

[a]Institució Catalana de Recerca i Estudis Avançats at Instituto de Biología Molecular de Barcelona (IBMB–CSIC), Jordi Girona 18-26, 08034 Barcelona, Spain, [b]Department of Biological Chemistry, John Innes Centre, Norwich NR4 7UH, England, and [c]Lehrstuhl für Strukturchemie, Tammannstrasse 4, Universität Göttingen, 37077 Göttingen, Germany

Correspondence e-mail: uson@ibmb.csic.es

Received 21 March 2007
Accepted 28 August 2007

NovP is an *S*-adenosyl-L-methionine-dependent *O*-methyltransferase from *Streptomyces spheroides* (subunit MW = 29 967 Da). Recombinant N-terminally His-tagged NovP crystallizes in space group *P*2, with approximate unit-cell parameters $a = 51.81$, $b = 46.04$, $c = 61.22$ Å, $\beta = 105.0^\circ$, giving a solvent content of 44% for a single copy of the His-tagged protomer per asymmetric unit. Native synchrotron data to a resolution of 1.35 Å were combined with three other native data sets collected at lower resolution (both in-house and at the synchrotron) for the sake of completeness and better scaling. Data to 2.45 Å resolution were subsequently recorded in-house from a single mercury derivative. Three partial mercury sites could be located with *SHELXD*, but the resulting phases had a mean error of about 81° and in our hands did not yield an interpretable map using standard automated software. Nevertheless, the structure of NovP could be solved by first tracing a small part of the structure by hand and then extrapolating within and beyond the experimental resolution limit using the 'free lunch algorithm' in *SHELXE*. The resulting phases have a mean phase error of 17° relative to a refined model.

1. Introduction

Experimental phasing of macromolecules has become increasingly efficient in recent years owing to advances both in hardware, leading to better data quality, and in the development of more sophisticated software that is able to extract and extend phases from very little starting information. Nevertheless, limited experimental data resolution is an unavoidable feature in macromolecular crystallography that negatively affects the structure-solution process. In addition, a number of common problems frequently exacerbate the situation even when proper care has been given to data collection and processing. These include a lack of completeness in the data owing to intrinsic low symmetry of the crystals and the limitations of a single-axis scan, radiation damage, anisotropy or lack of isomorphism between native and derivative data sets. All of these may hinder the process of phase extension and density modification, often resulting in failure of the structure solution despite success in the determination of the substructure. In particular, the barrier imposed by a lack of atomic resolution has been most resilient and approaches that will work well with data at resolutions beyond 1.2 Å stop being effective with lower resolution data sets (Morris & Bricogne, 2003). The atomicity constraint is very powerful either in reciprocal or real space but is dependent on atomic resolution. Thus, phase refinement or phase extension using the tangent

Table 1
Summary of X-ray data for NovP.

Values in parentheses are for the outer resolution shell. All statistics are based on data with the Friedel mates not merged, except for the native data to 1.35 Å, for which they were merged. The space group was *P*2 for all data sets.

Data set	Native, 1.35 Å	Native, 2.07 Å	Native, 2.14 Å	Native, 1.90 Å	Mercury derivative
Source	PX10.1	PX10.1	PX10.1	In-house	In-house
Wavelength (Å)	1.488	2.070	2.269	1.5418	1.5418
Rotation range (°)	150 (to 2.46 Å), 150 (to 1.35 Å)	507	720	720	360
Unit-cell parameters					
a (Å)	51.81	51.77	51.78	51.62	51.67
b (Å)	46.04	45.99	46.08	45.94	46.21
c (Å)	61.22	61.11	61.17	61.11	61.21
β (°)	105.0	105.0	105.0	104.8	104.6
Resolution range (Å)	36.3–1.35 (1.45–1.35)	27.4–2.07 (2.2–2.07)	20.9–2.13 (2.25–2.13)	22.3–1.9 (2.0–1.9)	27.5–2.45 (2.54–2.45)
Unique reflections	54942	15790	15438	21797	9977
Completeness (%)	89.0 (63.8)	92.0 (85.7)	98.2 (93.0)	98.7 (96.3)	95.5 (75.0)
Redundancy	3.3	10.2	13.4	13.5	5.8
$R_{\rm merge}$†	0.057 (0.173)	0.050 (0.177)	0.033 (0.074)	0.078 (0.291)	0.110 (0.418)
$\langle I/\sigma(I)\rangle$	15.5 (3.5)	33.4 (8.3)	30.4 (14.6)	24.2 (5.9)	13.8 (2.0)
Wilson *B* value (Å^2)	17.7	15.0	31.3	19.7	47.4
$R_{\rm iso}$‡	—	0.076	0.066	0.074	0.155

† $R_{\rm merge} = \sum|I - \langle I\rangle|/\sum I$, where I is the intensity of a reflection and $\langle I\rangle$ is the mean intensity of a group of equivalent reflections. ‡ $R_{\rm iso} = \sum(|F_{\rm PH} - F_{\rm P}|)/\sum|F_{\rm P}|$, the mean fractional isomorphous change between the 1.35 Å native amplitudes ($F_{\rm P}$) and amplitudes from the other data sets ($F_{\rm PH}$).

formula (Karle & Hauptman, 1956) or the minimal function (Miller *et al.*, 1993) can be very effective, while interpreting the maxima of a noisy map at atomic resolution as atomic positions (*i.e.* peak picking and peak-list optimization; Sheldrick & Gould, 1995) pushes the phases towards the right solution. At lower resolution, the partial interpretation of the map in terms of secondary-structure main-chain elements, as a way of introducing stereochemical information, is an effective way to extend phases to higher resolution if this chain tracing is sufficiently accurate (Perrakis *et al.*, 1999).

An elegant solution to the problem of insufficient resolution is simply to invent the data that could not be measured and to use density-modification techniques to extrapolate the phases to these unmeasured data! The first successful implementation of this idea, in the program *ACORN*, was described by Eleanor Dodson at the Phabio Meeting in Martina Franca, Italy in 2001. Two recent papers by the Bari group (Caliandro *et al.*, 2005*a*,*b*) and a paper on *ACORN* (Jia-xing *et al.*, 2005) have subsequently confirmed that both moduli and phases can be extrapolated effectively to a higher resolution than was accessible experimentally. Remarkably, the application of density modification including the extrapolated data leads to an improvement in the phase estimates of the observed reflections and thus to better interpretability of the corresponding electron-density maps. Even greater improvement is obtained when the extrapolated data are included in map calculation: the apparent resolution of the map is higher than the experimental resolution.

The proposed strategy has been incorporated into the program *SHELXE* (Sheldrick, 2002) and named the 'free lunch algorithm', as it is not obvious where the claimed improvement comes from: one appears to be getting something for nothing. The phases for the reflections that had not been measured are calculated by density modification exactly as described by Sheldrick (2002). The extrapolated amplitudes (and also those of missing lower resolution reflections) are those obtained from Fourier transformation of the density-modified map, normalized to fit an extrapolated Wilson plot.

Here, we report the structure solution at 1.35 Å of NovP, a previously unknown protein containing 262 amino acids. NovP is an *S*-adenosyl-L-methionine-dependent *O*-methyltransferase from *Streptomyces spheroides* that is responsible for the methylation of the 4′-hydroxyl group of the noviose sugar in the antibiotic novobiocin (Freel Meyers *et al.*, 2004). The crystallization and collection of a native X-ray data set have already been reported (Stevenson *et al.*, 2007). In this case, the application of the free lunch algorithm in combination with partial tracing using main-chain α-helix and β-strand fragments made the difference between solving or not solving the structure.

2. Materials and methods

2.1. Sample preparation

Recombinant NovP from *S. spheroides* was overexpressed, purified and crystallized as described previously (Stevenson *et al.*, 2007). Crystals were obtained from 2 *M* ammonium sulfate in 100 m*M* HEPES buffer pH 7.0 containing 1 m*M* *S*-adenosyl-L-homocysteine (SAH) and were cryoprotected using a brief soak (<30 s) in this crystallization solution supplemented with 25%(*v*/*v*) ethylene glycol in place of an equivalent volume of buffer (Garman & Schneider, 1997). A mercury derivative was prepared by soaking a crystal for 1 min in crystallization solution containing 10 m*M* mercury acetate. This crystal was cryoprotected as for native crystals but with the addition of 1 m*M* mercury acetate to the cryoprotectant. The crystals belong to space group *P*2, with $V_{\rm M}$ = 2.19 Å^3 Da^{-1} and a corresponding solvent content of 43.9% (Matthews, 1968) for a single copy of the His-tagged monomer per asymmetric unit (32 130 Da). Crystals were routinely transferred from one solution to another and were ultimately

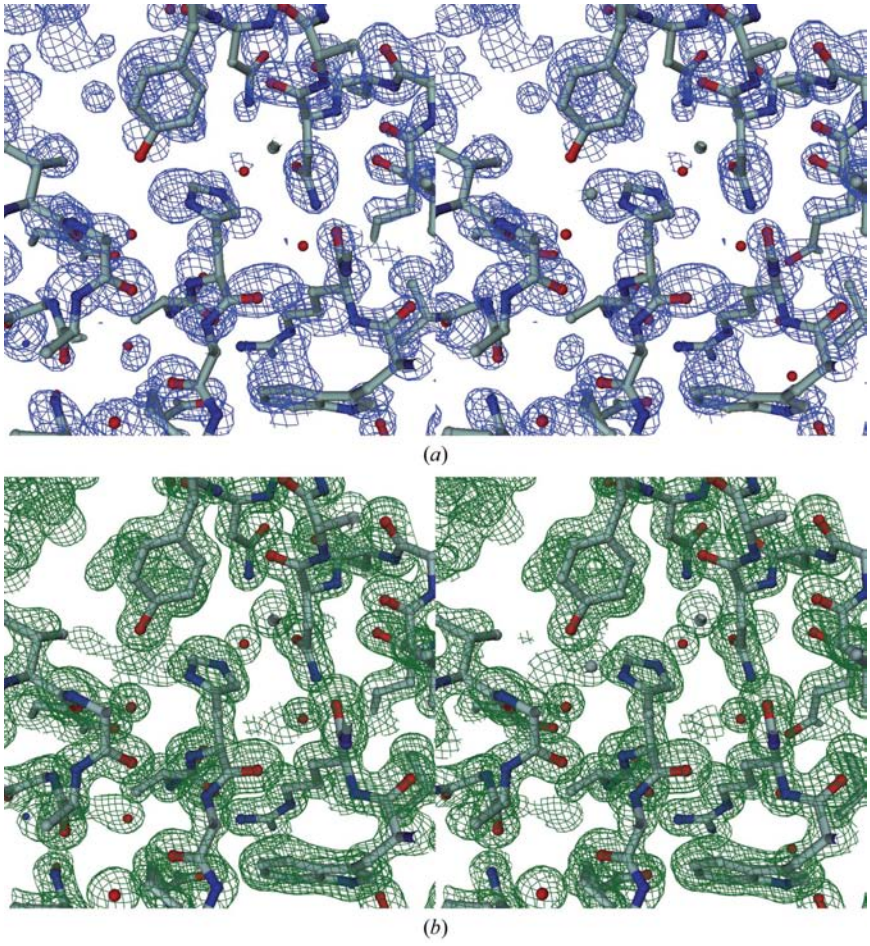

Figure 1
Maps of the same region of the structure calculated with (*a*) experimental phases from SIRAS and hand fitting of some secondary-structure elements followed by standard density modification with *SHELXE* to 1.35 Å (MapCC 0.57) and (*b*) after extension to 1.0 Å with virtual data (MapCC 0.94). This diagram was prepared using *DINO* (http://www.dino3d.org).

mounted for X-ray data collection using cryo-loops (Hampton Research).

2.2. X-ray data collection

For synchrotron data collection, the crystals were flash-cooled by plunging them into liquid nitrogen and stored prior to transport to the synchrotron. All three synchrotron data sets were collected using native crystals on station PX10.1 at the Daresbury Synchrotron Radiation Source. Crystals were transferred to the goniostat using Hampton Research cryo-tools and maintained at 100 K using a Cryojet cryocooler (Oxford Instruments). Diffraction data were recorded using a MAR225 CCD detector (MAR USA) with the wavelength set to 1.488 Å for the highest resolution data set and to longer wavelengths (2.070 and 2.269 Å, respectively) for two additional crystals, data from which were collected to 2.07 and 2.14 Å resolution, respectively.

For the two in-house data collections, crystals were flash-cooled and maintained at 100 K using an X-Stream cryocooler (Rigaku-MSC) and X-ray data were recorded on a MAR345 image-plate detector (X-ray Research) mounted on a Rigaku RU-H3RHB rotating-anode X-ray generator (operated at 50 kV and 100 mA) fitted with Osmic confocal optics and a copper target (Cu $K\alpha$; λ = 1.5418 Å). A further highly redundant native data set was collected to 1.9 Å resolution to enhance the completeness at low resolution and to improve the scaling of the synchrotron data sets. To this end, two 360° φ scans were performed on the same crystal. The mercury-derivative data set was collected in-house to 2.45 Å resolution in a single 360° φ scan using the equipment setup described above. The synchrotron data were processed using *HKL*-2000 and the in-house data were processed using *HKL* v.1.97 (Otwinowski & Minor, 1997). Preliminary data analysis and scaling were performed with *XPREP* (Sheldrick, 1990). Statistics for the various native data sets and the mercury derivative are summarized in Table 1.

2.3. Structure solution

Analysis of the NovP sequence using the *FUGUE* server (http://www-cryst.bioc.cam.ac.uk/~fugue/prfsearch.html; Shi *et al.*, 2001) indicated that there were no suitable templates for molecular replacement in the Protein Data Bank: although three weak hits were identified (with Z scores ranging from 11.4 to 9.3), their sequence identities with NovP did not exceed 18%. Attempts to solve the structure by molecular replacement using the deposited coordinates of catechol *O*-methyltransferase (PDB code 1vid; Vidgren *et al.*, 1994) as a search model did not succeed. Thus, a heavy-atom derivative was prepared as the next attempt to solve the NovP structure. In-house data from a mercury acetate soak gave a weak anomalous signal with $R_{\rm anom} = 100\sum|\langle I^+\rangle - \langle I^-\rangle|/\sum(\langle I^+\rangle + \langle I^-\rangle)/2 = 7.80\%$ and $R_{\rm p.i.m.} = 100\sum[1/(N-1)]^{1/2} \times \sum|I - \langle I\rangle|/\sum I = 3.56\%$. Usually an $R_{\rm anom}/R_{\rm p.i.m.}$ ratio of 1.5 is considered to be the minimum for successful phasing (Weiss *et al.*, 2001; Mueller-Dieckmann *et al.*, 2005), so the phasing power of these data is limited but should be sufficient; the mercury sites were probably only partially occupied. Three partial mercury sites with relative occupancies of 1:0.5:0.2 were found with *SHELXD* (Sheldrick *et al.*, 2001) using the SIRAS data truncated to 3.5 Å. Initial phases for the merged native data set were obtained using *SHELXE* (Sheldrick, 2002). We were not successful in solving the structure directly from these SIRAS phases with standard autotracing packages or with the then released version of *SHELXE*; apparently, the resulting phases were not of sufficient quality to allow a model to be built, the mean phase error being 80.7°. Nevertheless, at low resolution the discrimination between solvent and protein

regions together with the appearance of helix-like or strand-like density allowed us to place the model of catechol *O*-methyltransferase (PDB code 1vid) in the experimental map manually in a way that packed reasonably. This model could not be successfully refined, so it was used as a guide for placing secondary-structural elements by hand in the very noisy density of the SIRAS map; 109 residues comprising four polyalanine α-helices and seven β-strands were placed in this way and optimized by real-space refinement. The model phases were combined with the SIRAS phases and input to *SHELXE*. The resulting map (Fig. 1*a*) was clearly better, but was still not readily interpretable. When the *SHELXE* job was repeated with the free lunch algorithm to extrapolate data and phases to 1.0 Å, the improvement in map quality was dramatic and most of the side chains could have been assigned correctly without knowledge of the sequence (Fig. 1*b*).

The density modification and data extrapolation were performed with an improved version of the program *SHELXE* that has since been released as version 2006/3. The program *XtalView* (McRee, 1999) was used for graphical interpretation, real-space refinement and phase combination. For the purpose of calculating mean phase errors for the various phasing attempts, the traced model including 239 amino acids, the SAH ligand, two sulfate anions and 221 water molecules at full occupancy and with no disorder modelled was refined isotropically against all experimental data (*i.e.* without the use of a free *R* set or resolution cutoffs) in the merged native data set using the program *SHELXL* (Sheldrick & Schneider, 1997). All mean phase errors reported here are calculated relative to this model for the measured reflections only. A full refinement of a more complete model is in progress and will be published later.

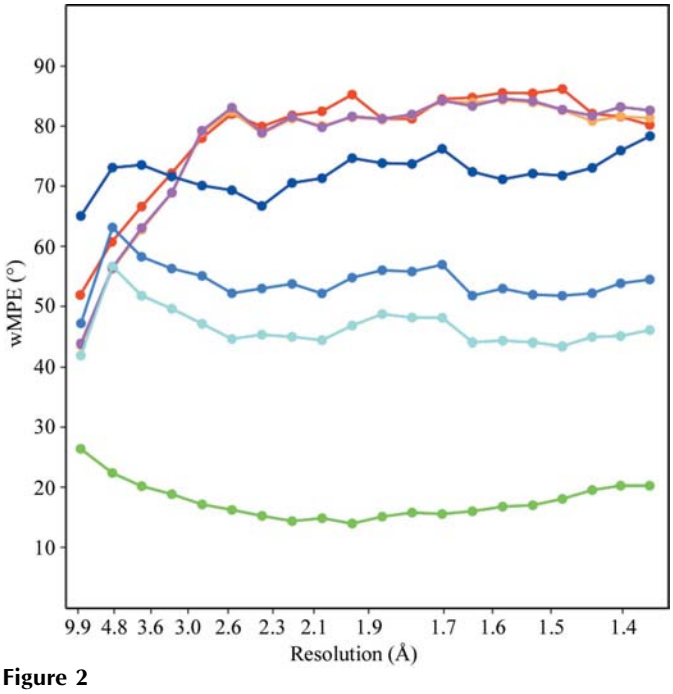

Figure 2
Plot of mean phase error weighted by $|F_o|$ and the figure of merit (MPE) *versus* resolution for the varioius attempts to solve the structure of NovP. The red line shows standard *SHELXE* phasing through SIRAS using the merged native data and the mercury derivative. The dark yellow line shows the same with missing data filled in to 1.35 Å and the magenta line with extrapolation to 1.0 Å; the phase errors are very similar and close to random except at resolutions lower than 3 Å for these three cases, although there is a small improvement at low resolution for the 1.0 Å extrapolation that we find difficult to explain. The dark blue line shows phases derived from polyalanine β-strand and α-helix fragments hand fitted into the SIRAS map after real-space refinement. For the medium blue line the SIRAS phases were combined with phases from the partial trace and then density-modified without data extrapolation, resulting in much better phases than from either source alone. For the light blue line the same procedure was performed with missing data filled in to 1.35 Å and for the green line with data extrapolation to 1.0 Å. The full 1.0 Å extrapolation results in a dramatic improvement in the MPE and map quality.

3. Results and discussion

A high-resolution native data set was collected from a single NovP crystal in two passes, the first to 2.46 Å and the second to a maximum resolution of 1.35 Å (Stevenson *et al.*, 2007). These data were essentially complete to 1.4 Å resolution (98.8% overall, 89.5% in the outer shell), but a significant number of additional reflections were recorded to 1.35 Å resolution (see Table 1) and were also used here. Two further native synchrotron data sets were collected to resolutions of almost 2 Å at longer wavelengths in an attempt to maximize the anomalous signal of the S atoms present in the protein (eight methionines and four cysteines in the wild-type sequence) and the SAH ligand. Nevertheless, this did not yield a data set leading to location of the S atoms. Finally, in-house native data were carefully collected to a resolution of 1.9 Å. All these native data were combined with the high-resolution data set to improve as much as possible the completeness (and redundancy) of the data in the inner resolution shells. Indeed, the data set obtained after merging all four native data sets is, but for five reflections at very low resolution, 100% complete to a resolution of 1.98 Å. The $R_{\rm merge}$ on combining the four native data sets (themselves already merged as in Table 1) is 0.075 and the overall $R_\sigma = \sum \sigma(F_o^2)/\sum F_o^2$ for the combined data is 0.027 (Friedel mates not merged) and 0.020 (Friedel mates merged).

Derivative data were collected to a maximum resolution of 2.45 Å from a crystal soaked in mercury acetate. A total of 360 × 1° oscillation images were recorded, yielding a data set that was 95.5% complete (see Table 1). Unfortunately, the lack of isomorphism between the native and derivative is acute for the shells at resolutions beyond 3.5 Å. The substructure solution with *SHELXD* using SIRAS clearly succeeds in locating three sites with relative occupancies of 1:0.5:0.2, even when less effort is devoted to the completeness and scaling of the native data set: any of the native data sets combined with the mercury derivative shows a clear solution for an equivalent set of sites.

Fig. 2 shows a plot of the weighted mean phase error *versus* resolution for the various strategies for structure solution and Fig. 3 displays maps of the same region in the central β-sheet calculated both with data truncated to 3.5 Å resolution and with data extrapolated to 1.0 Å. The red line in Fig. 2 shows the standard SIRAS approach using the best heavy-atom

substructure obtained with the program *SHELXD* and the combined native data for density modification with *SHELXE*. As can be appreciated from Fig. 2, the resulting phases are somewhat better at low resolution, where native and derivative are most isomorphous, but density modification is not succeeding in extending phases to higher resolution, despite the extremely high resolution of the native data. The MPE (mean phase error weighted by $|F_o|$ and the figure of merit) is 80.7°. The yellow line shows the results when missing data are filled in by extrapolation to the experimental resolution limit of 1.35 Å: the MPE (79.6°) is scarcely improved. The magenta line describes the outcome when data beyond the experimental resolution limit and up to 1.0 Å are included in the density-modification procedure starting from the same SIRAS phases. Although the overall improvement in the MPE is small, it is remarkable that most improvement is at low resolution, given that most of the additional extrapolated data are at atomic resolution.

The dark blue line shows the results of density modification starting from phases derived from polyalanine fragments of

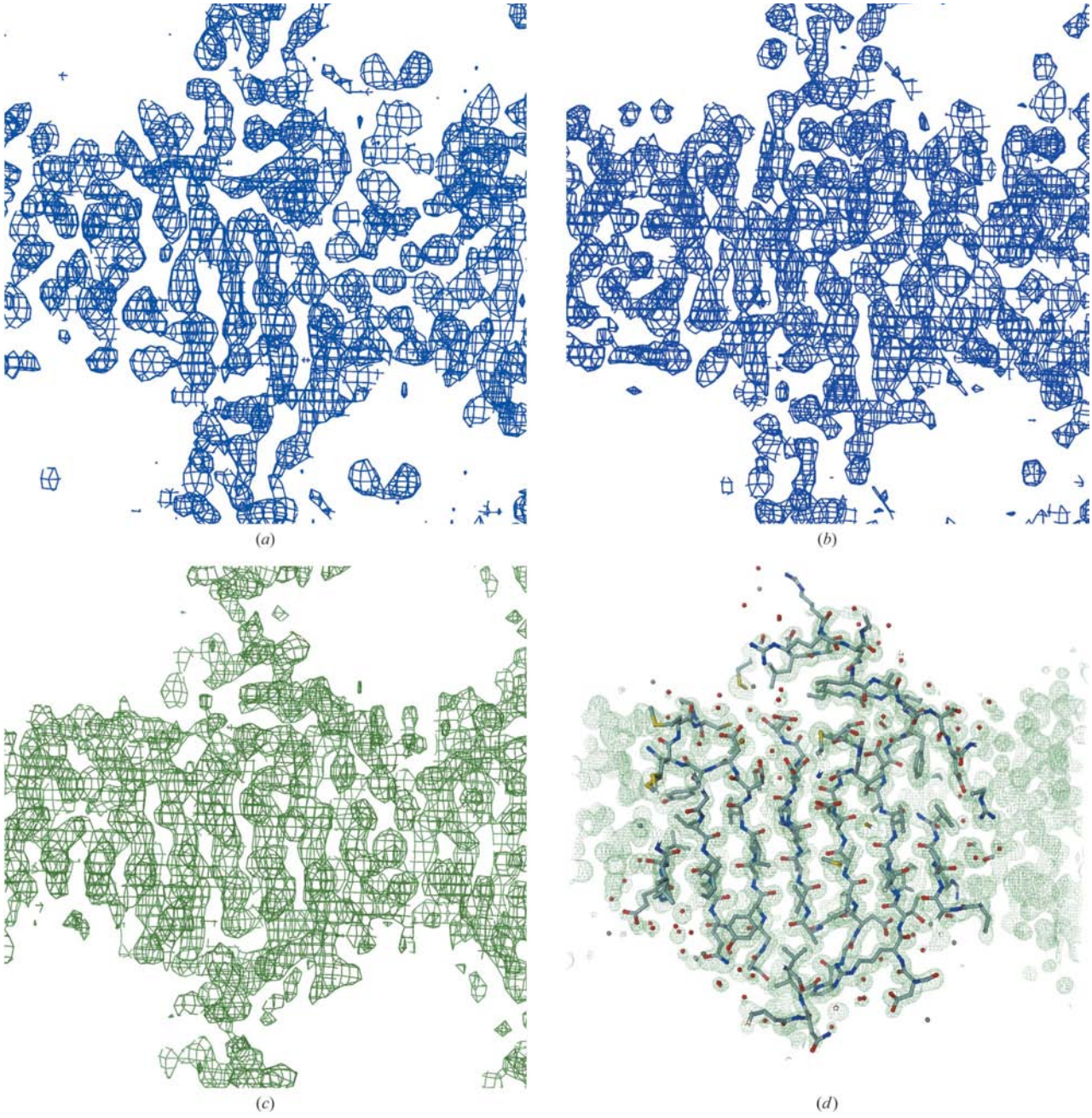

Figure 3
Experimental FOM-weighted maps of the same region of the central β-sheet from the following calculations: (*a*) SIRAS map after density modification using data to 3.5 Å, (*b*) SIRAS map after density modification and extrapolation to 1.0 Å, (*c*) SIRAS combined with partial tracing and extrapolated to 1.0 Å but then truncated to 3.5 Å and (*d*) SIRAS combined with partial tracing extrapolated to 1.0 Å. The final model is also displayed in Fig. 3(*d*). These diagrams were prepared using *DINO* (http://www.dino3d.org).

four α-helices and seven β-strands, making a total of 109 residues, fitted and real-space refined against the map corresponding to the magenta line. At low resolution the phases are worse than those derived from the SIRAS data alone, but exhibit a roughly constant MPE of 67.4° throughout the full resolution range. The medium blue line plots the results of density modification on a combination of the original SIRAS phases with phases derived from the main-chain fragments of the α-helices and β-strands interpreted into the map. Partial tracing of the SIRAS-derived map followed by combination of the SIRAS and partial structure phases results in a significant improvement throughout the resolution range as the MPE falls to 54.0°. The light blue line shows what happens when missing data to 1.35 Å are extrapolated: a further 10° improvement in the MPE is observed. It is the final combination of the SIRAS experimental phases, partial tracing and data extrapolation to 1.0 Å that makes the most significant difference and brings the MPE down to only 17.0° (Fig. 1*b*). The resultant phases were of more than sufficient quality to enable automatic building of the structure using *ARP*/*wARP* (Perrakis *et al.*, 1999): a total of 238 residues of the 262 amino-acid native sequence were fitted to the electron density at 1.4 Å resolution. When the refinement has been completed the structure will be deposited in the PDB.

4. Conclusions

In the case of this structure, the combination of partial tracing and data extrapolation makes all the difference between obtaining an interpretable map or not, *i.e.* between solving or not solving the structure. Either of these approaches alone has a beneficial effect on the mean phase error, but the combination of both is much more powerful. Partial tracing should be beneficial as it imposes a constraint on the map that incorporates stereochemical information and atomicity. We appreciate that our suggestion that there may still be cases where human intervention can have a decisive impact on phasing is rather like saying (a few years ago) that a grandmaster would beat a computer at chess; it will not be long before autotracing pipelines solve this structure too!

Less apparent is why exploiting extrapolated data that have been derived from the available map should be beneficial in the density-modification process and lead to a genuine improvement in the phasing. Our experience with other structures suggests that data extrapolation almost always produces a modest improvement of a few degrees in the phases and in a few cases such as this one the MPE improves by more than 30°, provided that the experimental data extend to at least 2.0 Å. Apparently, one is obtaining something for nothing (*i.e.* a 'free lunch'). Possible explanations include the following.

(i) The algorithm corrects Fourier truncation errors that may have had a more serious effect on the maps than generally realised.

(ii) Phases are more important than amplitudes, so as long as the extrapolated phases are correct, the tolerance towards the accuracy of the extrapolated amplitudes will be large.

(iii) Zero is a very poor estimate of the amplitude of a reflection that we did not measure, so that it is easy to improve on it.

Finally, great care was taken in obtaining the best possible experimental native data. Given the low symmetry of the crystals, the high-resolution data collected from a single-axis scan at the synchrotron were not complete. To improve the completeness and redundancy of the native data set, all available data including in-house data were combined. Although the data extrapolation apparently compensates for the weak starting phase information, it probably benefits from having the best possible experimental data.

IU and GMS are grateful to the European Union Integrated Project BIOXHIT for support. IU thanks the Spanish MEC for financial support (grant BIO2003-06653). CEMS and DML would like to acknowledge the BBSRC for financial support through responsive mode funding (ref. B19400) and the Core Strategic Grant to the John Innes Centre. GMS thanks the Fonds der Chemischen Industrie for support. We are also grateful to M. Cianci, M. Ellis and R. Strange for assistance with data collection at the SRS (Daresbury).

References

Caliandro, R., Carrozzini, B., Cascarano, G. L., De Caro, L., Giacovazzo, C. & Siliqi, D. (2005*a*). *Acta Cryst.* D**61**, 556–565.
Caliandro, R., Carrozzini, B., Cascarano, G. L., De Caro, L., Giacovazzo, C. & Siliqi, D. (2005*b*). *Acta Cryst.* D**61**, 1080–1087.
Freel Meyers, C. L., Oberthür, M., Xu, H., Heide, L., Kahne, D. & Walsh, C. T. (2004). *Angew. Chem. Int. Ed. Engl.* **43**, 67–70.
Garman, E. F. & Schneider, T. R. (1997). *J. Appl. Cryst.* **30**, 211–237.
Jia-xing, Y., Woolfson, M. M., Wilson, K. S. & Dodson, E. J. (2005). *Acta Cryst.* D**61**, 1465–1475.
Karle, J. & Hauptman, H. (1956). *Acta Cryst.* **9**, 635–651.
McRee, D. E. (1999). *J. Struct. Biol.* **125**, 156–165.
Matthews, B. W. (1968). *J. Mol. Biol.* **33**, 491–497.
Miller, R., DeTitta, G. T., Jones, R., Langs, D. A., Weeks, C. M. & Hauptman, H. A. (1993). *Science*, **259**, 1430–1433.
Morris, R. J. & Bricogne, G. (2003). *Acta Cryst.* D**59**, 615–617.
Mueller-Dieckmann, C., Panjikar, S., Tucker, P. A. & Weiss, M. S. (2005). *Acta Cryst.* D**61**, 1263–1272.
Otwinowski, Z. & Minor, W. (1997). *Methods Enzymol.* **276**, 307–326.
Perrakis, A., Morris, R. M. & Lamzin, V. S. (1999). *Nature Struct. Biol.* **6**, 458–463.
Sheldrick, G. M. (1990). *SHELXTL Software Package for the Determination of Crystal Structures*, Release 6.12. Bruker AXS Inc., Madison, WI, USA.
Sheldrick, G. M. (2002). *Z. Kristallogr.* **217**, 644–650.
Sheldrick, G. M. & Gould, R. O. (1995). *Acta Cryst.* B**51**, 423–431.
Sheldrick, G. M., Hauptman, H. A., Weeks, C. M., Miller, R. & Usón, I. (2001). *International Tables for Crystallography*, Vol. *F*, edited by M. G. Rossmann & E. Arnold, pp. 333–345. Dordrecht: Kluwer Academic Publishers.
Sheldrick, G. M. & Schneider, T. R. (1997). *Methods Enzymol.* **277**, 319–343.
Shi, J., Blundell, T. L. & Mizuguchi, K. (2001). *J. Mol. Biol.* **310**, 243–257.
Stevenson, C. E. M., Freel Meyers, C. L., Walsh, C. T. & Lawson, D. M. (2007). *Acta Cryst.* F**63**, 236–238.
Vidgren, J., Svensson, L. A. & Liljas, A. (1994). *Nature (London)*, **368**, 354–358.
Weiss, M. S., Sicker, T. & Hilgenfeld, R. (2001). *Structure*, **9**, 771–777.